CELL DEATH

Flotillin-mediated endocytosis and ALIX–syntenin-1–mediated exocytosis protect the cell membrane from damage caused by necroptosis

Weiliang Fan[1,2], Jia Guo[1,2], Beichen Gao[1,2], Wenbin Zhang[1,2], Liucong Ling[1,2], Tao Xu[1,2], Chenjie Pan[1,2], Lin Li[1,2], She Chen[1,2], Hua Wang[3,4], Jing Zhang[3,5], Xiaodong Wang[1,2]*

Necroptosis is a form of regulated necrosis that is implicated in various human diseases including Alzheimer's disease. Necroptosis requires the translocation of the pseudokinase MLKL from the cytosol to the plasma membrane after its phosphorylation by the kinase RIPK3. Using protein cross-linking followed by affinity purification, we detected the lipid raft–associated proteins flotillin-1 and flotillin-2 and the ESCRT-associated proteins ALIX and syntenin-1 in membrane-localized MLKL immunoprecipitates. Phosphorylated MLKL was removed from membranes through either flotillin-mediated endocytosis followed by lysosomal degradation or ALIX–syntenin-1–mediated exocytosis. Thus, cells undergoing necroptosis need to overcome these independent suppressive mechanisms before plasma membrane disruption can occur.

INTRODUCTION

In response to the activation of tumor necrosis factor receptors (TNFRs), mammalian cells can activate multiple signaling pathways, including pathways that cause cell death through either apoptosis or necrosis (*1*). One such form of necrotic cell death, necroptosis, occurs if the abundance of the cellular inhibitor of apoptosis antagonist Smac (also known as Diablo) is high and the activity of apoptosis-causing caspase-8 is relatively low (*2*–*4*). Necroptosis can thus be robustly induced by the combination of TNFα, a small molecule that mimics Smac protein function, and a pan-caspase inhibitor (*5*). Such a treatment activates the receptor-interacting protein kinase RIPK1, which then recruits the related kinase RIPK3 through interactions between their respective RIP homotypic interaction motif regions, resulting in RIPK3 activation (*5*–*7*). Activated human RIPK3, as marked by the phosphorylation of its Ser^{227} site, recruits and phosphorylates its substrate, the mixed lineage kinase domain-like protein MLKL, which is a pseudokinase that normally has its pseudokinase domain folded in a conformation that prevents its N-terminal helix bundle from targeting membranes (*8*–*10*). RIPK3-mediated phosphorylation of human MLKL at Thr^{357} and Ser^{358} located in its pseudokinase domain relieves the inhibitory effect of the pseudokinase domain, thus allowing the activated phospho-MLKL to oligomerize and translocate from the cytosol to membranes (including the plasma membrane) to cause membrane disintegration resulting in necrosis (*11*–*13*).

RESULTS

What happens to phospho-MLKL once it reaches the membrane during necroptosis has not been fully clarified. To study this issue, we first characterized the composition of MLKL-associated protein complex from the membrane microdomains called lipid rafts, onto which phospho-MLKL can localize (*12*). Lipid rafts are resistant to nonionic detergent and thus can be purified from other membrane fractions by centrifugation after a nonionic detergent wash (*14*). We used human colon cancer HT-29 cells in which we knocked down endogenous MLKL and stably expressed MLKL fused with a 3xFlag-HA (hemagglutinin) tagged to its C terminus. These cells were incubated with dithiobis(succinimidyl propionate) (DSP), a primary amine-reactive and membrane-permeable cross-linker after necroptosis was induced with TNFα, Smac mimetics, and zVAD-FMK (hereafter referred to as TSZ), as previously described (*5*, *8*). The lipid raft fractions from these cells were subjected to two-step affinity purification using Flag and HA antibodies (Fig. 1A). The success of cross-linking manifested as a smeared Flag signal with slower mobility in SDS–polyacrylamide gel electrophoresis (SDS-PAGE) gels run under nonreducing conditions; the smear collapsed into a discrete band when a reducing agent (β-mercaptoethanol) was included in the sample loading buffer (fig. S1A). The Flag signal only appeared in the lipid raft fraction after TSZ treatment (fig. S1A). The successful isolation of lipid rafts was marked by the enrichment of the known lipid raft–residing proteins such as flotillin and caveolin (fig. S1A).

Silver staining of the final protein elute showed, in addition to the bait protein (MLKL–3xFlag-HA) and the heavy/light chains of the antibodies, several discrete protein bands, which were further identified by mass spectrometry as being flotillin-1, flotillin-2, ALIX, and syntenin-1, respectively (Fig. 1B and data file S1). Flotillins are lipid raft–residing proteins, which contain an N-terminal prohibitin homology domain responsible for membrane binding and a C-terminal α-helical region required for oligomerization to form heterotetramers (*15*). Functions of flotillins include cell signal transduction, cell-cell contact regulation, membrane-cytoskeletal interaction, and clathrin-independent endocytosis (*16*–*18*). Syntenin-1 is a PDZ domain–containing protein that binds to the C-terminal cytosolic end of various transmembrane proteins and that facilitates signal transduction mediated by these proteins. For instance, syntenin-1 facilitates exosome formation through interaction with syndecan (*19*–*22*). ALIX (also known as programmed cell death 6–interacting protein)

[1]National Institute of Biological Sciences, Beijing, No. 7 Science Park Road, Zhongguancun Life Science Park, Beijing 102206, China. [2]Tsinghua Institute of Multidisciplinary Biomedical Research, Tsinghua University, Beijing 102206, China. [3]Department of Pathology, School of Basic Medical Sciences, Peking University Health Science Center, Beijing 100191, China. [4]Department of Pathology, Peking University Third Hospital, Beijing 100191, China. [5]Department of Pathology, University of Washington School of Medicine, Seattle, WA, USA.
*Corresponding author. Email: wangxiaodong@nibs.ac.cn

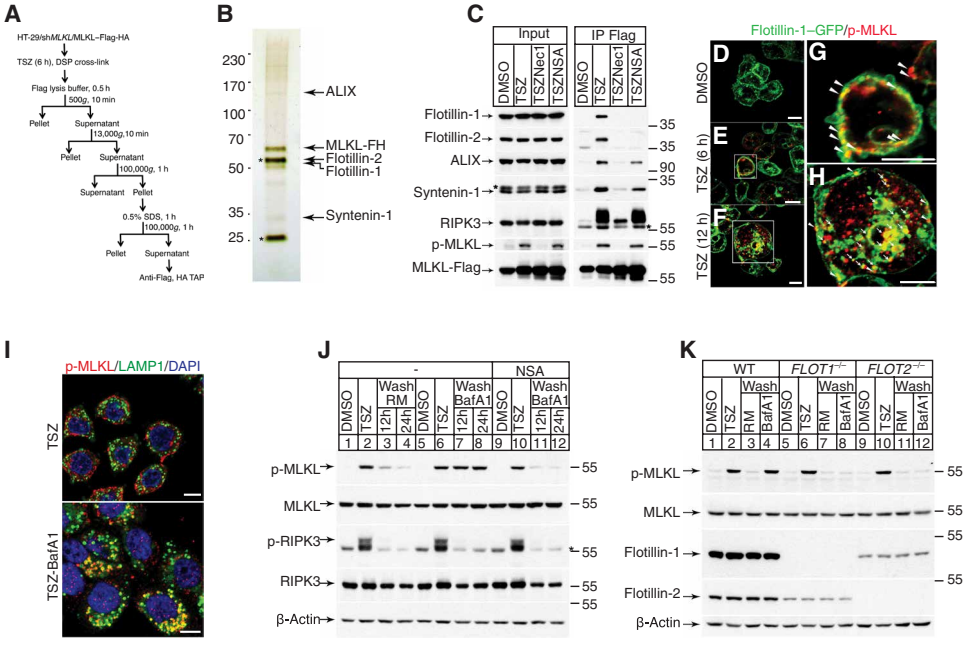

Fig. 1. Flotillins mediated the relocalization of phospho-MLKL from cell membranes to lysosomes. (**A**) Procedures for the cross-linking and tandem affinity purification of the lipid raft–bound phospho-MLKL protein complex. TSZ, TNFα (20 ng/ml), Smac mimetic (100 μM), and z-VAD (20 μM); DSP, dithiobis(succinimidyl propionate) (2 mM); TAP, tandem affinity purification. (**B**) Phospho-MLKL protein complexes collected as described in (A) were denatured, separated by SDS-PAGE, and silver stained. Several discrete bands were excised and identified by proteomics, as indicated. Antibody heavy and light chains were labeled with asterisks (*). FH, 3xFlag-HA. $n = 2$ independent experiments. (**C**) HT-29/sh*MLKL*/Flag-MLKL cells were treated with dimethyl sulfoxide (DMSO), TSZ, TSZ+Nec-1 (necrostatin-1) (20 μM), and TSZ+NSA (necrosulfonamide) (1 μM) for 6 hours, cross-linked with DSP, lysed in SDS-containing buffer, and subjected to Flag agarose immunoprecipitation (IP). The immunocomplexes were analyzed by Western blotting analysis using the indicated antibodies. $n = 2$ independent experiments. (**D** to **H**) HT-29 cells stably expressing FLOT1-EGFP (enhanced green fluorescent protein) were treated with DMSO or TSZ for 6 hours, then fixed, and labeled with phospho-MLKL antibody and Alexa Fluor 647 secondary antibody. The arrowheads point to colocalization of phospho-MLKL and flotillin-1 on cell membranes; the arrows point to colocalization of phospho-MLKL and flotillin-1 on the membranes of intracellular vesicles. $n = 2$ independent experiments. Scale bars, 20 μm. (**I**) HT-29 cells were treated with TSZ for 6 hours (TSZ) and then cultured in bafilomycin A1–containing medium for 12 hours (TSZ-BafA1). Cells were immunolabeled with phospho-MLKL and LAMP1 (lysosome-associated membrane protein 1) antibodies and Alexa Fluor 647 (red) and Alexa Fluor 514 (green) secondary antibodies, respectively. $n = 3$ independent experiments. Scale bars, 20 μm. DAPI, 4′,6-diamidino-2-phenylindole. (**J**) HT-29 cells were treated with DMSO (lanes 1 and 5) or with TSZ (lanes 2 and 6) for 6 hours. TSZ-treated HT-29 cells were further cultured in fresh medium (RM; lanes 3 and 4) or in medium containing bafilomycin A1 (BafA1; 20 nM) for 12 hours (lane 7) or for 20 hours (lane 8). Cells in lanes 9, 10, 11, and 12 were also treated with NSA (1 μM). $n = 3$ independent experiments. (**K**) Wild-type HT-29, HT-29/*FLOT1*$^{-/-}$, and HT-29/*FLOT2*$^{-/-}$ cells were treated with DMSO or TSZ for 6 hours. TSZ-treated cells were further cultured in fresh medium (RM) or in bafilomycin A1 (BafA1)–containing medium for 20 hours. Cells were immunoblotted as indicated. $n = 3$ independent experiments.

is an ESCRT (endosomal sorting complexes required for transport) accessory protein that promotes membrane abscission during cytokinesis, damaged membrane repair, viral budding, and exosome formation (*22*–*25*).

The associations between MLKL with the abovementioned proteins were confirmed by coimmunoprecipitation and Western blotting (Fig. 1C). TSZ induced the interaction of phospho-MLKL with all four proteins, and these interactions were blocked when the upstream kinase RIPK1 was inhibited by Nec-1, indicating the requirement of active necroptosis for these interactions to happen. However, when cells were cotreated with NSA (*8*), a chemical inhibitor that prevents MLKL from translocating to membranes (*13*), only the association with flotillin-MLKL but not those with ALIX or syntenin-1 was blocked, suggesting that the association between flotillins with MLKL required membrane targeting of MLKL, whereas ALIX and syntenin-1 bound to MLKL before it reaches membranes.

Flotillin-1–GFP ectopically expressed in HT-29 cells appeared as discrete punctae either on cell membranes or in the cytosol, which represent lipid raft microdomains and intracellular endosomes, respectively (Fig. 1D). Upon 6 hours after application of TSZ (a time point before necroptosis begins), MLKL was phosphorylated and the phospho-MLKL signal also appeared as punctae on cell membranes and in the cytosol, locations that overlapped with those of flotillin-1–GFP (Fig. 1, E to H).

We then asked whether phospho-MLKL is eventually directed to lysosomes. When HT-29 cells were treated with TSZ for 6 hours, little phospho-MLKL colocalized with lysosomes decorated by LAMP1 (Fig. 1I, top, and fig. S1B). However, when the cells were switched to fresh medium containing bafilomycin A1 (*26*), an H^+–adenosine triphosphatase inhibitor that blocks lysosome acidification, much of the phospho-MLKL signal was found within the lumen of lysosomes (Fig. 1I, bottom, and fig. S1B).

To directly test whether phospho-MLKL was degraded in lysosomes, we treated HT-29 cells with TSZ for 6 hours and then continuously cultured them for 12 or 20 hours in fresh medium. Western blotting showed that phospho-MLKL levels decreased in a time-dependent manner after the cells were switched to the fresh medium (Fig. 1J, lanes 1 to 4). However, when cells were cultured in fresh medium containing bafilomycin A1 after 6 hours of TSZ treatment, cellular phospho-MLKL did not change even 20 hours after TSZ induction, indicating that blocking lysosomal degradation stabilized phospho-MLKL (Fig. 1J, lanes 5 to 8). Moreover, when cells were cotreated with NSA, which prevents phospho-MLKL from reaching membranes (*8*, *13*), cellular phospho-MLKL was reduced after the cells were switched to fresh medium despite the presence of bafilomycin A1 (Fig. 1J, lanes 9 to 12). These results suggested that lysosomal degradation required that phospho-MLKL reach cell membranes, where it was endocytosed followed by endolysosome fusion. In contrast, the phospho-RIPK3 signal disappeared after the cells were switched into fresh medium for 12 hours, and the disappearance was not affected by either bafilomycin A1 or NSA (Fig. 1J), indicating that phospho-RIPK3 was resolved by a different pathway while cells recovered from necroptotic insult.

Because flotillins associate with phospho-MLKL upon TSZ treatment and because they function in endocytosis, we asked whether flotillins mediated the transportation of phospho-MLKL from the cell membrane to lysosomes. Flotillin-1 and flotillin-2 are two closely related proteins that form heterotetramers in lipid rafts. The tetramerization is essential for the stability of both proteins (*27*). Knockout of *FLOT1* (which encodes flotillin-1) led to major reduction of flotillin-2 protein in the cell, and knockout of *FLOT2* (which encodes flotillin-2) caused a substantial reduction in flotillin-1 protein level as well (Fig. 1K). We found that when either *FLOT1* or *FLOT2* was knocked out, phospho-MLKL still disappeared in TSZ-treated cells that were subsequently switched to fresh medium (Fig. 1K, lanes 3, 7, and 11). However, bafilomycin A1 prevented the degradation of phospho-MLKL only in parental HT-29 cells but not in cells lacking either flotillin (Fig. 1K, lanes 4, 8, and 12). This result suggested that flotillins were required for the lysosomal degradation of phospho-MLKL, and when flotillins were absent, an alternative mechanism was required to remove phospho-MLKL from necroptotic cells in a lysosome-independent manner.

Because the N-terminal helix bundle of MLKL is essential for its ability to target and disrupt membranes (*9*–*13*), we then tested the role of the N terminus of MLKL in its lysosomal degradation. We replaced the first four α helices of the MLKL protein with a different phospholipid-binding motif, the pleckstrin homology (PH) domain from human phospholipase C–δ (PLC-δ) protein, to generate a chimeric protein that we named PLC-δ–MLKL (fig. S2A). The PH domain binds to phosphatidylinositol 4,5-bisphosphate on the inner layer of plasma membranes (*28*). Confocal microscopy of HT-29 cells indicated that PLC-δ–MLKL was constitutively associated with plasma membranes, and immunoblotting revealed that this chimeric protein was phosphorylated by RIPK3 upon necroptosis induction (fig. S2, B and C). We treated a cell line that simultaneously expressed PLC-δ–MLKL and endogenous MLKL at comparable levels with TSZ and monitored the levels of the phosphorylated forms of both proteins. Endogenous phospho-MLKL was degraded after fresh medium exchange after 6 hours of TSZ treatment (fig. S2C, lane 2), and this degradation was blocked by either bafilomycin A1 or chloroquine (*29*), a compound that neutralizes lysosomal pH (fig. S2C, lanes 3 and 4). In contrast, phospho–PLC-δ–MLKL was not degraded after medium exchange, and its level was not affected by either the presence of lysosomal inhibitors or knockdown of *FLOT2*, a manipulation that rendered the degradation of phospho-MLKL insensitive to bafilomycin A1 or chloroquine (fig. S2C, lanes 6 to 8). Consistently, the chimeric PLC-δ–MLKL did not interact with flotillins, as measured by coimmunoprecipitation assays (fig. S2D). These results suggest that the lysosomal degradation of phospho-MLKL is facilitated through the interaction between the flotillins and the N-terminal helix bundle of membrane-bound MLKL molecules.

To determine whether the flotillin-mediated lysosomal degradation of the phospho-MLKL pathway identified in HT-29 cells applied to other cell lines, we tested the phospho-MLKL in several other RIPK3-expressing colon cancer cell lines. SW620 and WiDr cells showed lysosomal degradation of phospho-MLKL that was sensitive to *FLOT2* knockdown (Fig. 2A and fig. S3A). In contrast, in HCT-8 cells, the degradation of phospho-MLKL was insensitive to bafilomycin A1 regardless of the presence or absence of flotillin-2 (Fig. 2B). Sequencing the genomic DNA encompassing the *FLOT1* and *FLOT2* genes revealed the occurrence of a C-to-T point mutation within one allele of the *FLOT1* gene, leading to a leucine-to-proline change at position 380 in the cytosolic region of flotillin-1 (Fig. 2C). To test whether this L380P mutation was responsible for the loss of lysosomal degradation of phospho-MLKL, we transfected wild-type flotillin-1 or the L380P version in HCT-8 cells in which the endogenous flotillin-1 was knocked down by short hairpin RNA (shRNA). Reintroduction of wild-type flotillin-1, but not the L380P version, restored lysosomal degradation of phospho-MLKL (Fig. 2D). To further confirm that the lack of lysosomal degradation of phospho-MLKL in HCT-8 cells was due to the L380P mutation in flotillin-1, we also used CRISPR-Cas9 technology to edit the C-to-T change of *FLOT1* gene back to the wild-type sequence and found that this gene edit restored the lysosomal degradation of phospho-MLKL (Fig. 2E).

We further explored the molecular basis for the observed loss of lysosomal degradation activity in cells harboring the L380P alteration in flotillin-1. We reintroduced either Flag-tagged wild-type flotillin-1 or L380P version in HT-29 cells in which the endogenous *FLOT1* was knocked out. We then treated the cells with the cross-linker DSP and immunoprecipitated flotillin-1 with Flag antibody. Similar amounts of Flag signal and flotillin-2 were precipitated in cells treated with DMSO or TSZ, confirming that flotillin-1 and flotillin-2 form a stable complex regardless of necroptosis induction (Fig. 2F). On the other hand, MLKL coimmunoprecipitated with flotillin-1 only when cells were undergoing necroptosis (Fig. 2F). However, the L380P flotillin-1 mutant showed reduced association with phospho-MLKL compared with wild-type flotillin-1 under necroptosis-inducing conditions (Fig. 2F), suggesting that the region around Leu^{380} likely contains the motif required for the association of flotillin-1 with phospho-MLKL.

The ability of a single C-to-T change in one *FLOT1* gene copy to render cells unable to degrade phospho-MLKL in lysosomes suggested that such a change is dominant negative in nature. Consistently, ectopic expression of the L380P form of flotillin-1 in HT-29 cells diminished the lysosomal degradation of phospho-MLKL and sensitized cells to TSZ-induced necroptosis. In contrast, ectopic expression of wild-type flotillin-1 in HT-29 cells had little impact (Fig. 2, G and H).

The human *FLOT1* gene bears many single-nucleotide polymorphisms (SNPs), some of which are located around Leu^{380}. We tested each of the eight SNPs that flank the Leu^{380} site to affect the ability of flotillin-1 to interact with phospho-MLKL and to counter necroptosis. Flotillin-1 with four of these eight SNPs—A375V, V381L, S382F, and S385I—showed compromised association with phospho-MLKL (fig. S3B). HT-29/*FLOT1*$^{-/-}$ cells expressing any of these four forms of *FLOT1* were more sensitive to necroptosis induction compared to that expressing the wild-type *FLOT1* (fig. S3C). These results suggest that the presence of Pro at position 380 in flotillin-1 in HCT-8 cells is also a result of SNP.

Because flotillins are lipid raft–residing proteins, the association between flotillins and phospho-MLKL could be responsible for targeting phospho-MLKL to lipid rafts. To test this hypothesis, we knocked down flotillin-2 in HT-29 cells and found that both flotillin-1 and flotillin-2 were reduced in lipid raft fractions to nearly undetectable levels (Fig. 2I, lanes 7 to 12). A substantial fraction of phospho-MLKL was located in the lipid raft fraction after necroptosis induction (Fig. 2I, lane 6). Knockdown of flotillin-2 resulted in the retention of phospho-MLKL in the non–lipid raft fraction (Fig. 2I, lanes 11 and 12), suggesting that the lipid raft association of phospho-MLKL depends on the presence of flotillins in lipid rafts.

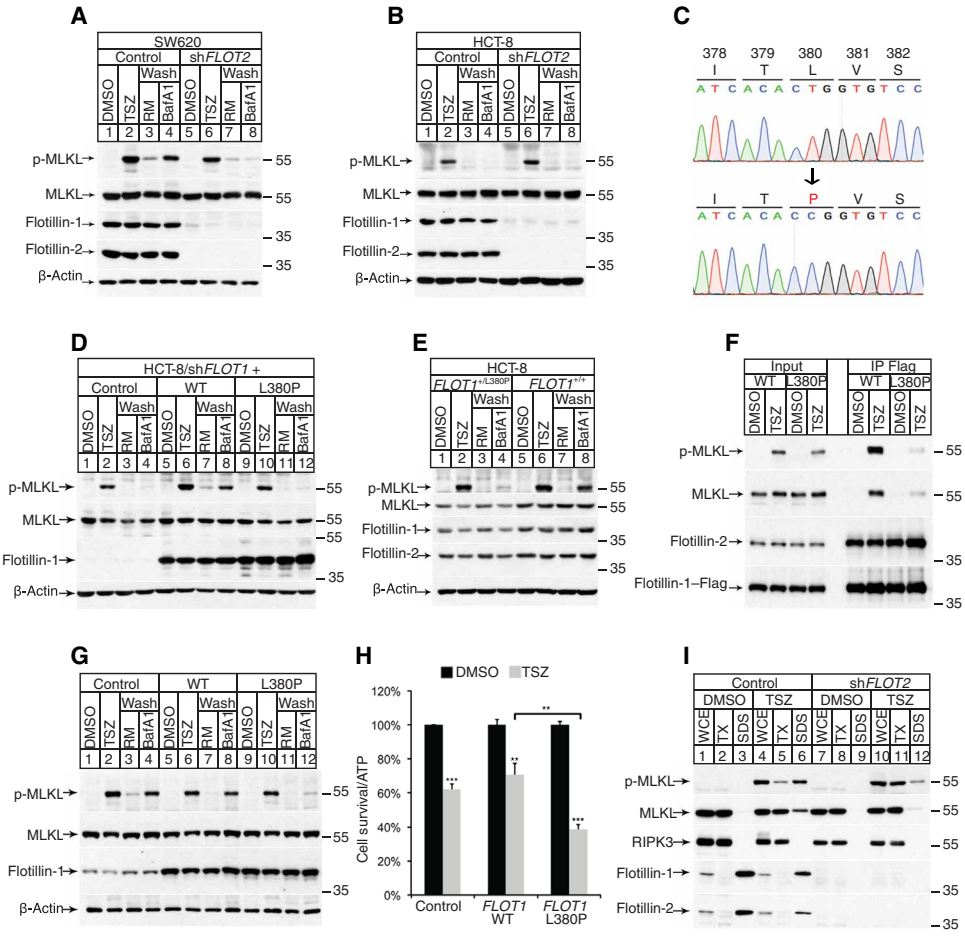

Fig. 2. Binding between the N-terminal helix bundle of phospho-MLKL and a C-terminal region of flotillin-1 was required for flotillin-mediated endocytosis of phospho-MLKL. (**A**) SW620 and SW620/sh*FLOT2* cells were treated with DMSO or TSZ for 6 hours. TSZ-treated cells were further cultured in fresh medium (RM) or bafilomycin A1–containing medium (BafA1) for 20 hours. Cells were immunoblotted as indicated. $n = 2$ independent experiments. (**B**) HCT-8 and HCT-8/sh*FLOT2* cells were treated with DMSO or TSZ for 6 hours. TSZ-treated cells were further cultured in fresh medium (RM) or bafilomycin A1–containing medium (BafA1). Cells were immunoblotted as indicated. $n = 2$ independent experiments. (**C**) Genomic sequence showing a mutation of the *FLOT1* gene that causes a leucine-to-proline mutation at position 380 in HCT-8 cells. $n = 3$ independent experiments. (**D**) HCT-8/sh*FLOT1* cells stably expressing vector, *FLOT1*, or *FLOT1* L380P were treated with DMSO or TSZ for 6 hours. TSZ-treated cells were further cultured in fresh medium (RM) or bafilomycin A1–containing medium (BafA1) for 20 hours. Cells were immunoblotted as indicated. $n = 2$ independent experiments. WT, wild type. (**E**) HCT-8/$FLOT1^{+/L380P}$ (wild type) and HCT-8/$FLOT1^{+/+}$ (edited by CRISPR-Cas9) were treated with DMSO or TSZ for 6 hours. TSZ-treated cells were further cultured in fresh medium (RM) or bafilomycin A1–containing medium (BafA1) for 20 hours. Cells were immunoblotted as indicated. $n = 2$ independent experiments. (**F**) HT-29/$FLOT1^{-/-}$ cells stably expressing wild-type *FLOT1*-Flag or *FLOT1* L380P-Flag were treated with DMSO or TSZ for 6 hours. Cells were cross-linked with DSP and subjected to Flag immunoprecipitation. The purified protein complexes were immunoblotted as indicated. $n = 2$ independent experiments. (**G**) HT-29 cells or HT-29 cells overexpressing wild-type *FLOT1* or *FLOT1* L380P were treated with DMSO or TSZ for 6 hours. TSZ-treated cells were further cultured in fresh medium (RM) or bafilomycin A1–containing medium (BafA1). Cells were immunoblotted as indicated. $n = 2$ independent experiments. (**H**) HT-29 cells or HT-29 cells overexpressing wild-type *FLOT1* or *FLOT1* L380P were treated with DMSO or TSZ for 20 hours. Cell survival was measured with the CellTiter-Glo assay. Data represent means ± SD from three independent experiments. $^{**}P \leq 0.01$ and $^{***}P \leq 0.001$, two-way analysis of variance (ANOVA) followed by post hoc Tukey's test. ATP, adenosine 5′-triphosphate. (**I**) HT-29 or HT-29/sh*FLOT2* cells were treated with either DMSO or TSZ for 6 hours. Whole-cell extract (WCE), Triton X-100 soluble fraction (TX), and Triton X-100 insoluble but SDS soluble fraction (SDS) were collected and immunoblotted as indicated. $n = 2$ independent experiments.

exocytosed in an ESCRT-dependent fashion (*30*–*32*) and because the other two membrane MLKL-interacting proteins identified in this study were ALIX and syntenin-1 (Fig. 1B), both of which are involved in regulating the ESCRT-dependent exocytosis of membrane-bound proteins (*25*), we therefore tested whether these two proteins participated in regulating the exocytosis of phospho-MLKL. Knockout of either *ALIX* or *SDCBP* (which encodes syntenin-1) reduced the levels of phospho-MLKL in the exosome fractions collected from the culture medium of TSZ-treated cells (Fig. 3A). In contrast, knockout of either *ALIX* or *SDCBP* did not affect the lysosomal degradation of phospho-MLKL (Fig. 3B). Moreover, knockout of either *FLOT1* or *FLOT2* did not affect the presence of phospho-MLKL in exosomes (Fig. 3C). These results suggested that flotillin-mediated lysosomal degradation and ALIX–syntenin-1–mediated exocytosis of phospho-MLKL were independently regulated processes. Consistent with this notion, we observed that although individual knockout of *FLOT2*, *ALIX*, or *SDCBP* sensitized HT-29 cells to necroptosis (Fig. 3D and fig. S4A), concomitant knockout of *FLOT2* and *ALIX* or *FLOT2* and *SDCBP* rendered cells more sensitive to necroptosis induced by TSZ as measured by both propidium iodide staining of cells and a membrane leakage assay using CytoTox-Glo (Fig. 3, D and E; fig. S4B; and movie S1). In contrast, the time course of phosphorylation of inhibitor of nuclear factor κBα (IκB) in response to TNFα treatment in the *FLOT2*/*SDCBP* double-knockout cells was similar to that of wild-type parental cells, suggesting that TNFR signaling was not enhanced (fig. S5).

Knockdown of the ESCRT-I subunit protein TSG101 (tumor susceptibility gene 101) [also known as VPS23 (vacuolar protein sorting 23)] prevented the exocytosis of phospho-MLKL (Fig. 3F), further confirming that ALIX–syntenin-1–mediated exocytosis of phospho-MLKL depended on the ESCRT pathway. The N-terminal, ubiquitin-binding UEV (ubiquitin E2 variant) domain was required for TSG101 to promote the exocytosis of phospho-MLKL because a TSG101 mutant lacking the UEV domain was unable to rescue the defective exocytosis and accelerated necroptosis caused by TSG101 knockdown (Fig. 3, F and G). The N-terminal helix bundle of MLKL was also required for its exocytosis because the PLC-δ–MLKL

Because phospho-MLKL still disappeared in the absence of flotillins, we sought to identify the flotillin-independent pathway responsible for removal of phospho-MLKL. Because phospho-MLKL can be

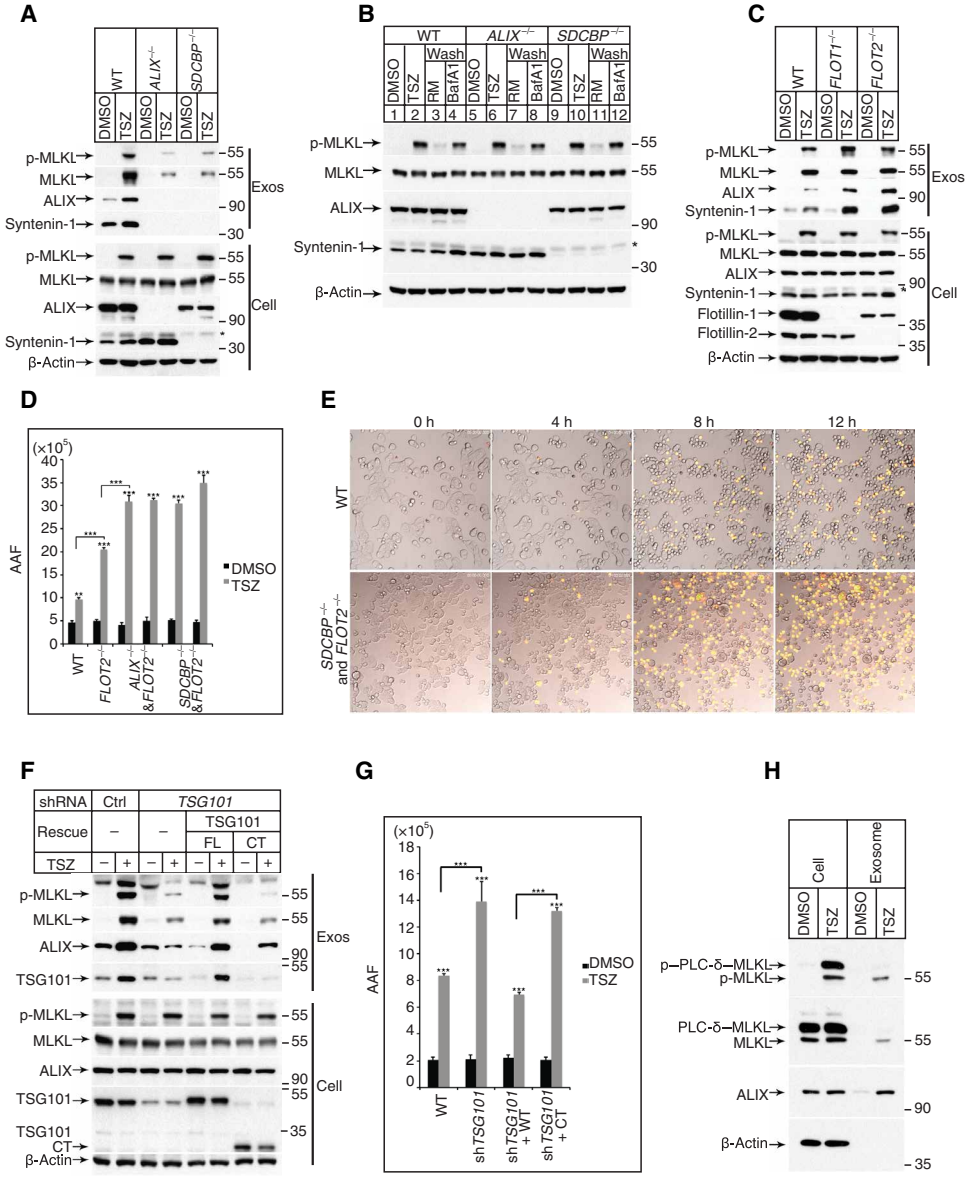

Fig. 3. ALIX and syntenin-1–mediated exocytosis of phospho-MLKL. (**A**) Wild-type HT-29, HT-29/*ALIX*$^{-/-}$, and HT-29/*SDCBP*$^{-/-}$ cells were treated with DMSO or TSZ for 6 hours. Cells and exosomes (Exos) were immunoblotted as indicated. $n = 2$ independent experiments. (**B**) Wild-type HT-29, HT-29/*ALIX*$^{-/-}$, and HT-29/*SDCBP*$^{-/-}$ cells were treated with DMSO or TSZ for 6 hours. TSZ-treated cells were further cultured in fresh medium (RM) or bafilomycin A1–containing medium (BafA1) for 20 hours. Cells were immunoblotted as indicated. $n = 2$ independent experiments. (**C**) Wild-type HT-29, HT-29/*FLOT1*$^{-/-}$, and HT-29/*FLOT2*$^{-/-}$ cells were treated with DMSO or TSZ for 6 hours. Cells and exosomes were immunoblotted as indicated. $n = 2$ independent experiments. (**D**) Wild-type HT-29, HT-29/*FLOT2*$^{-/-}$, HT-29/*FLOT2*$^{-/-}$/*ALIX*$^{-/-}$, and HT-29/*FLOT2*$^{-/-}$/*SDCBP*$^{-/-}$ cells were treated with DMSO or TSZ for 20 hours. Cell death was measured with the CytoTox-Glo cytotoxicity assay. Data represent means ± SD from three independent experiments. $^{**}P \leq 0.01$ and $^{***}P \leq 0.001$, ANOVA followed by post hoc Tukey's test. (**E**) Wild-type HT-29 and HT-29/*FLOT2*$^{-/-}$/*SDCBP*$^{-/-}$ cells were treated with TSZ for 16 hours; cell membrane disruption was visualized with propidium iodide staining. $n = 3$ independent experiments. (**F**) HT-29, HT-29/sh*TSG101*, and HT-29/sh*TSG101* cells expressing either full-length TSG101 (FL) or a C-terminal truncated form of TSG101 (146aa-end) (CT) were treated with DMSO or TSZ for 6 hours. Cells and exosomes were immunoblotted as indicated. $n = 2$ independent experiments. (**G**) HT-29, HT-29/sh*TSG101*, and HT-29/sh*TSG101* cells expressing either full-length TSG101 or a C-terminal truncated form of TSG101 (146aa-end) were treated with DMSO or TSZ for 20 hours. Cell death was measured with the CytoTox-Glo cytotoxicity assay. Data represent means ± SD from three independent experiments. $^{***}P \leq 0.001$, two-way ANOVA followed by post hoc Tukey's test. (**H**) HT-29 cells ectopically expressing the chimeric protein PLC-δ–MLKL were treated with DMSO or with TSZ for 6 hours. Cells and exosomes were immunoblotted as indicated. $n = 2$ independent experiments. AAF, alanyl-alanyl-phenylalanyl-aminoluciferin.

chimera was not exocytosed in TSZ-treated cells (Fig. 3H). A protein fragment encompassing the N-terminal helix bundle of MLKL immunoprecipitated TSG101 as well as ALIX and syntenin-1 (fig. S6). Thus, ALIX and syntenin-1 mediate the exocytosis of phospho-MLKL, likely through an association with ESCRT complex proteins such as TSG101.

We then investigated whether these two phospho-MLKL–resolving mechanisms, the flotillin-mediated endocytosis and the ALIX–syntenin-1–mediated exocytosis, were conserved in mouse cells. In mouse L929 cells, we found that knockout of the *Flot2* but not of either *Alix* or *Sdcbp* enhanced necroptosis in response to TZ (TNFα+z-VAD-FMK) (fig. S7, A and B). Thus, the flotillin-mediated endocytosis of phospho-MLKL is conserved in mouse cells.

To test the impact of the flotillin-mediated regulation of necroptosis in animals, we generated FVB (Friend leukemia virus B) mice with a double knockout of *Flot1* (which encodes flotillin-1) and *Flot2* (which encodes flotillin-2). Similar to a previous report, these flotillin-null mice were born and developed without any obvious defects (*33*). We assessed necroptosis in bone marrow–derived macrophages (BMDMs) from 8-week-old flotillin-null and heterozygous mice exposed to TSZ or lipopolysaccharide (LPS) plus z-VAD; either treatment induces necroptosis in macrophages. Macrophages from flotillin-null mice died much faster than those isolated from heterozygous mice (Fig. 4A). Consistently, when the flotillin-null and their heterozygous littermates were injected with TNFα plus z-VAD to induce systemic inflammatory response syndrome (SIRS) (*34*), 10 of 13 (77%) flotillin-null mice met the end point of the mortality assay within the first 12 hours. In contrast, only one of nine heterozygous mice treated with the same amount of TNFα and z-VAD met the end point of the mortality assay within the same time frame. Moreover, all flotillin-null mice survived TNFα/z-VAD–induced SIRS when co-injected with the RIPK1 inhibitor RIPA-56 (*35*), confirming that the accelerated death in flotillin-null mice resulted from enhanced necroptosis (Fig. 4B).

Necroptosis has been reported to be induced in the neurons of patients with Alzheimer's disease (*36*), and endolysosomal function is often impaired in these

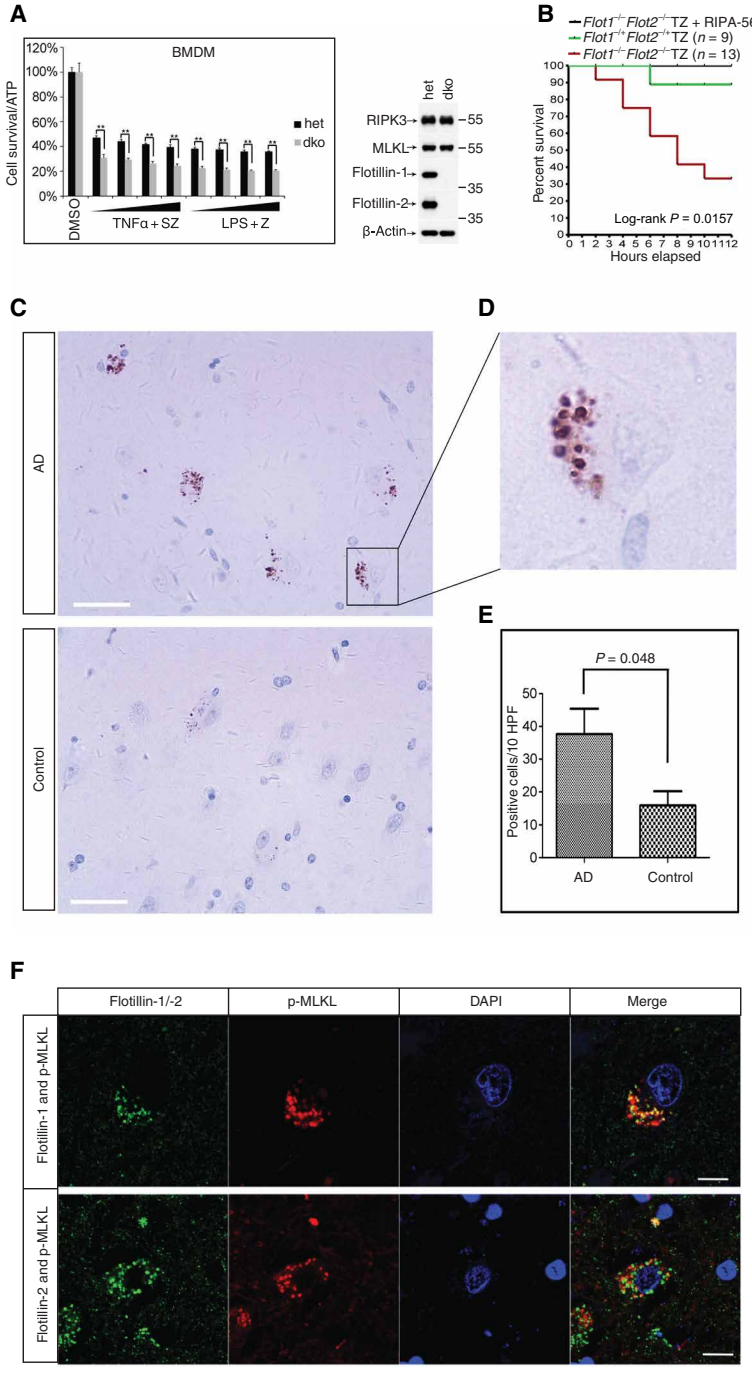

Fig. 4. Flotillin-mediated endocytosis of phospho-MLKL attenuated necroptotic damage in mice and may occur in human Alzheimer's disease. (**A**) BMDMs from *Flot1*$^{-/+}$ *Flot2*$^{-/+}$ and *Flot1*$^{-/-}$ *Flot2*$^{-/-}$ mice were treated with TNFα (50, 10, 2, or 0.4 ng/ml) with Smac mimetic and z-VAD, or LPS (100, 20, 4, or 0.8 ng/ml) with z-VAD for 20 hours. Cell survival was measured with the CellTiter-Glo assay. $n = 3$ mice per genotype. $^{**}P \leq 0.01$, two-way ANOVA followed by post hoc Tukey's test. het, heterozygous; dko, double knockout. (**B**) Survival curves for *Flot1*$^{-/+}$ *Flot2*$^{-/+}$ and *Flot1*$^{-/-}$ *Flot2*$^{-/-}$ mice injected with mouse TNFα (5.5 μg) and z-VAD (20 μM) (TZ) in the presence or absence of RIPA-56 (1 μM). $P = 0.0157$, log-rank test. (**C**) Hippocampal sections from Alzheimer's disease (AD) and control patients were labeled with a phospho-MLKL antibody. Representative of five patients from AD and eight people from the control group. Scale bars, 20 μm. (**D**) Higher magnification image from (C). (**E**) Quantitation of phospho-MLKL–positive cytosolic punctae from either patients with AD or the control group. HPF, high-power field. $P = 0.048$, Student's *t* test. (**F**) Hippocampal sections from human patients with AD costained for phospho-MLKL and flotillin-1 or anti–flotillin-2. Representative of five patients. Scale bars, 20 μm.

neurons, which results in the accumulation of lysosomal contents in the areas of the brain most strongly affected by the disease (*37*, *38*). We therefore tested whether phospho-MLKL and/or flotillin-1/2 also accumulated in the lysosomes of patients with Alzheimer's disease by staining hippocampal slices from autopsy samples. Compared to the hippocampal slices of age-matched normal individuals, those from patients with Alzheimer's disease had more prominent phospho-MLKL signals in the intracellular vesicles of the pyramidal neurons (Fig. 4, C to E). Furthermore, we noted that many of these phospho-MLKL–positive punctae were apparently colocalized with flotillins in the hippocampal slices from patients with Alzheimer's disease (Fig. 4F).

DISCUSSION

A major remaining question in necroptosis research is how necrotic cell death is executed and regulated once phospho-MLKL reaches the plasma membrane. Purified MLKL variants that either have phosphomimetic mutations or lack the inhibitory C-terminal pseudokinase domain can efficiently break artificial liposome membranes containing negatively charged phospholipids in vitro (*10*, *13*). Therefore, the N-terminal helix bundle of MLKL appears to have an intrinsic membrane-disrupting activity. However, consistent with previous reports, phospho-MLKL was observed at the plasma membrane hours after necroptosis induction (Fig. 1D), and cells can recover if the necroptosis-inducing agents are removed in time. Therefore, it must be necessary for active MLKL to overcome negative regulators before membrane disruption occurs. Various studies have previously indicated that the ESCRT pathway can remove phospho-MLKL–containing membrane vesicles from cells undergoing necroptosis, thereby attenuating this cell death process (*30*–*32*). The current study demonstrates that it is not one but two such regulatory pathways that counter the necroptotic function of phospho-MLKL. In addition to the ESCRT-mediated exocytosis mediated by MLKL-interacting ALIX and syntenin-1, flotillin-mediated endocytosis followed by lysosomal degradation is another major pathway that removes phospho-MLKL from the plasma membrane.

We believe that the interactions between phospho-MLKL and flotillins as well as the abovementioned ESCRT-associated proteins are not due to colocalization on specified membrane structures such as lipid rafts but rather due to specific protein-protein interactions. Knockout of flotillins was associated with the

loss of lipid raft localization of phospho-MLKL (Fig. 2I). Moreover, multiple single amino acid residue changes around the Leu^{380} site of flotillin-1 resulted in the loss of binding of phospho-MLKL to flotillins and the ability to remove phospho-MLKL from necroptotic cells (Fig. 2, A to H, and fig. S3, B and C). In addition, even when MLKL was prevented from reaching the plasma membrane by NSA treatment, ALIX and syntenin-1 but not flotillins still coimmunoprecipitated with phospho-MLKL (Fig. 1C). However, although our data are suggestive of a direct interaction between the flotillins and phospho-MLKL, we acknowledge that formal evidence is not included in the present study and can be addressed by in vitro binding assays using purified fragments of these proteins.

The associations between MLKL and these abovementioned proteins all required the intact N-terminal helix bundle of MLKL (figs. S2D and S6). Such associations may effectively interfere with the membrane-disrupting activity of MLKL and prevent necroptosis by removing phospho-MLKL from the membrane. Given the consequences of necrotic cell death, it is not unusual that cells have evolved efficient and redundant surveillance systems to ensure that any death signal being received is a true signal. Moreover, different cell types should be able to set their false-negative "tolerance level" for free phospho-MLKL through their multiple surveillance systems.

Thus, we favor the following model of necroptosis execution: Free phospho-MLKL accumulates to sufficient levels to cause direct membrane disruption. To do so, phospho-MLKL must first overcome these innate lines of defense before it can breach plasma membranes to drive necroptosis. This hypothesis does not rule out the presence of a binding partner for MLKL for necroptosis execution. Finding such putative coexecutioners may be facilitated by eliminating the phospho-MLKL–interacting proteins identified by this study.

Our observation of the colocalization of phospho-MLKL with flotillins in the intracellular vesicles of pyramidal neurons in patients with Alzheimer's disease, viewed alongside the role of necroptosis in Alzheimer's disease (*36*), may illustrate how such defense mechanisms, while being active in diseased tissue, can eventually be overcome by necroptosis-causing signals of increasing intensity.

MATERIALS AND METHODS

Cell lines, antibodies, DNA constructs, and other reagents

L929 and HT-29 cells have been previously described (*5*, *8*). The colon cancer cell lines SW620, WiDr, and HCT-8 were initially purchased from the American Type Culture Collection (ATCC) and cultured according to the ATCC's instructions. Cells were routinely tested for contamination. The antibodies used in this study include the following: phosphorylated human MLKL (Abcam, ab187091), phosphorylated mouse MLKL (Abcam, ab196436), human MLKL (Abcam, ab184718), mouse MLKL (Abgent, AP14272b), mouse RIPK3 (ProSci, 2283), RIPK1 [Cell Signaling Technology (CST), 3493], β-actin (MBL, PM053-7), LAMP1 (Santa Cruz Biotechnology, sc-20011), ALIX (Abcam, ab88388), syntenin-1 (Abcam, ab19903), flotillin-1 (BD Bioscience, 610821; CST, 3253), flotillin-2 (BD Bioscience, 610384; CST, 3244), and TSG101(Proteintech, 14497-1-AP). The rabbit anti-human RIPK3 polyclonal antibody was generated by immunizing rabbits with full-length RIPK3 recombinant protein and was used in our previous work (*5*, *8*). The following reagents were purchased from Sigma: chloroquine (Sigma-Aldrich, C6628) and bafilomycin A1 (Sigma-Aldrich, B1793), anti-Flag agarose (Sigma-Aldrich, A2220), and anti-HA agarose (Sigma-Aldrich, A2095). Guide RNAs used for CRISPR-mediated knockout included: *FLOT1*, GTCAGCCAATAAGATCACAC; *FLOT2*, GTGGGCAATTGCCACACGGT; *ALIX*, GCAGCTGAAAAAGACCTCAG; *SDCBP*, GCCTTCAAGTCTTCGAGAGA; *Flot2*, TGAGACCACCAGCGCCTCGT; *Alix*, GCAGTACTGCCGTGCGGCCG; and *Sdcbp*, GAATGCTTGGCTGGCGGGAT. The following shRNAs for lentivirally mediated knockdown were purchased from Sigma-Aldrich: *FLOT1* (TRCN0000353591), CCGGATAGCTGAAGTTGCCTGAATGCTCGAGCATTCAGGCAACTTCAGCTATTTTTTG; *FLOT2* (TRCN0000148873), CCGGCGTGTATGACAAAGTGGACTACT CGAGTAGTCCACTTTGTCATACACGTTTTTTG; and *TSG101* (TRCN0000315109), CCGGGCCTTATAGAGGTAATACATACTCGAGTATGTATTACCTCTATAAGGCTTTTTG. Concentrations of each of the reagents were as follows unless otherwise stated in the text: TNFα (20 ng/ml), Smac mimetic (100 nM), z-VAD (20 μM), bafilomycin A1 (20nM), and chloroquine (100 nM).

Human brain tissue samples

Formalin-fixed paraffin-embedded human brain autopsy specimens including five patients with Alzheimer's disease and eight age-matched controls were obtained from the University of Washington Neuropathology Core Brain Aging and Neurodegeneration Brain Bank. Alzheimer's disease was clinically and neuropathologically confirmed by applying current diagnostic standards. Specimens from the hippocampus were cut to a thickness of 4 μm and mounted on polylysine-coated slides.

Cell culture and transfection

Complementary DNA transfection was carried out using Lipofectamine 3000 (Life Technologies). To conduct shRNA-mediated gene silencing, pLKO.1 puro (Addgene, 8453) constructs containing 19–base pair gene-specific shRNAs were first packed into virus by cotransfecting 293T cells with psPAX2 and pMD2.G. Twenty-four hours after transfection, the lentivirus was collected, filtered through a 0.44-μm filter, and used to infect target cells. Forty-eight hours after infection, the virus-containing medium was removed and the target cells were selected using puromycin at the concentration of 10 μg/ml. Knockdown efficiency was confirmed by Western blotting.

Measuring cell survival and cell death

Cell survival was measured with CellTiter-Glo (Promega, G7570) luminescent viability assay according to the manufacturer's instructions. Membrane leakage of necroptotic cells was measured by CytoTox-Glo (Promega, G9292) luminescent assay according to the manufacturer's instruction. Briefly, cells were plated in 96-well culture plate at a concentration of 5000 per well 24 hours before the assay. After inducing necrosis, the plates were moved out of the incubator and allowed to reach room temperature. A total of 50 μl of either CellTiter-Glo or CytoTox-Glo reaction solution was added into each well and mixed with cell culture medium by pipetting. The reaction was carried out on a horizontal shaker at room temperature for 15 min. Luminescent signal was then measured in a plate reader (PerkinElmer, EnSpire). Necrotic cell death was also measured in live cells by applying propidium iodide in culture medium and capturing by spinning disk confocal microscope.

The generation of knockout mice and animal experiment protocols

FVB mice were purchased from Vital River Laboratory Animal Technology Co. and housed in a specific pathogen-free animal facility. *Flot1* and *Flot2* double-knockout mice were generated using the

CRISPR-Cas9 system with guide RNA sequence ggggtccccatctcagtcac (*Flot1*) or gtagcctgtgaacagttcct (*Flot2*). Experiments using the knockout mice were conducted by the animal facility of the National Institute of Biological Sciences, Beijing.

Mice with ages between 8 to 12 weeks were used for TNFα + zVAD–induced SIRS. Mice were injected intravenously with mTNFα (5.5 μg per mouse) and z-VAD (200 μg per mouse) diluted in phosphate-buffered saline (PBS). Humane end points were used in conducting the surviving experiments. Rectal temperature was recorded every 2 hours using a lubricated digital rectal thermometer. Mice with body temperature below 23°C or those that fail to evade handling were euthanized using inhaled anesthetic. All animal experiments were conducted following the Chinese Ministry of Health national guidelines for the housing and care of laboratory animals and performed in accordance with institutional regulations after review and approval by the Institutional Animal Care and Use Committee of the National Institute of Biological Sciences. The animal experiment was carried out in a blinded manner.

Culturing of BMDM

Eight-week-old mice were sacrificed by cervical dislocation, and both abdomen and hind legs of the mice were sterilized with 70% ethanol. Both tibias were isolated and cut at both ends. The bones were then flushed with PBS using a 5-ml syringe. The bone marrow cells were then passed through a 40-μm cell strainer. The collected cell suspensions were centrifuged at 1000*g* for 5 min. The cell pellets were resuspended Dulbecco's modified Eagle's medium containing 20% fetal bovine serum (FBS), 1% penicillin-streptomycin, and 30% (v/v) L929 conditioned medium and plated on cell culture plates. BMDMs were cultured in the L929 conditioned medium for 5 to 7 days to allow differentiation before performing cell death assays.

Cross-link and tandem affinity purification of MLKL from lipid raft

HT-29/sh*MLKL*/MLKL–3xFlag-HA cells were cultured to confluence of 80% in 60 of 15-cm culture dishes. Cells were treated with TNFα, Smac mimetic, and z-VAD for 6 hours before being collected by scraping. Cells were then centrifuged at 1000*g* for 10 min to remove culture medium. The collected cell pellet was washed with cold PBS three times to completely remove any residual culture medium. PBS containing 2 mM DSP cross-linker was then used to resuspend the cell pellet. The reaction was done at room temperature for 30 min before being quenched by tris-HCl buffer (pH 7.4) at a final concentration of 20 mM. Cells were then pelleted again and lysed on ice in Flag lysis buffer [150 mM NaCl, 20 mM tris-HCl (pH 7.4), 0.5% Triton X-100, protease inhibitor cocktail, and phosphatase inhibitor cocktail]. The cell suspension was centrifuged at 500*g* for 10 min, after which the supernatant was further centrifuged at 13,000*g* for 10 min. The resulting supernatant was then centrifuged again at 100,000*g* for 60 min. The pellet collected from this 100,000*g* centrifugation (P100) was then dissolved in Flag lysis buffer plus 0.5% SDS by rotating overnight to allow thorough lysis. The lysate was then centrifuged again at 100,000*g* for 60 min to remove any insoluble particles. The supernatant from the final centrifugation was collected, and SDS was added to a final dilution to 0.1% before the supernatant was used for Flag and HA affinity pull-down assays.

Cell lysates were incubated with 50 μl of anti-Flag agarose overnight at 4°C and washed with Flag lysis buffer three times before being eluted in Flag peptide (0.1 mg/ml) for 6 hours. The Flag elute was then incubated with 20 μl of anti-HA agarose overnight at 4°C before being washed three times again in Flag lysis buffer, followed by elution in HA peptide (0.5 mg/ml) for 6 hours. The final elute was then denatured by boiling for 10 min in 1× SDS protein loading buffer containing β-mercaptoethanol. It was then separated by SDS-PAGE followed by silver staining.

Mass spectrometric analysis

Protein bands from the SDS-PAGE gel after silver staining were destained and digested in gel with sequencing grade trypsin [trypsin (10 ng/μl) and 50 mM ammonium bicarbonate (pH 8.0)] overnight at 37°C. Peptides were extracted with 5% formic acid/50% acetonitrile and 0.1% formic acid/75% acetonitrile sequentially and then concentrated to ~20 μl. The extracted peptides were separated by an analytical capillary column (50 μm by 10 cm) packed with 5-μm spherical C18 reversed phase material (YMC, Kyoto, Japan). A Waters nanoACQUITY UPLC system (Waters, Milford, USA) was used to generate the following high-performance liquid chromatography gradient: 0 to 30% B in 60 min and 30 to 70% B in 15 min (A, 0.1% formic acid in water and B, 0.1% formic acid in acetonitrile). The eluted peptides were sprayed into a linear trap quadropole Orbitrap Velos mass spectrometer (Thermo Fisher Scientific, San Jose, CA, USA) equipped with a nano–electrospray ionization ion source. The mass spectrometer was operated in data-dependent mode with 1 mass spectrometry scan followed by 10 high-energy collisional dissociation tandem mass spectrometry scans for each cycle. Database searches were performed on an in-house Mascot server (Matrix Science Ltd., London, UK) against the International Protein Index human protein database.

Exosome collection

The FBS used to culture cells destined for exosome experiments was depleted of exosomes by centrifugation at 140,000*g* for 3 hours; the supernatant of the centrifuged FBS was then used for cell culture. HT-29 cells were treated with DMSO or TSZ for 6 hours. The culture medium of the cells was collected and centrifuged at 1000*g* for 10 min, the supernatant of which was then centrifuged again at 10,000*g* for 30 min. The resulting supernatant was centrifuged again at 140,000*g* for 3 hours. The pellets (P140) were directly lysed in 1× SDS loading buffer and analyzed by Western blotting.

Immunofluorescent staining

HT-29 cells were initially cultured on coverslips coated with polylysine. After treatment, the culture medium was aspirated and cells were washed once with PBS. Cells were fixed with 3.7% (w/v) of formaldehyde in PBS for 15 min at room temperature and permeabilized with prechilled methanol at −20°C for 10 min. The methanol was then removed, and the cells were washed three times with PBS at room temperature, for 10 min each time. Cells were then blocked with blocking buffer [bovine serum albumin (1 mg/ml) in PBS] at 37°C for 15 min. After blocking, cells were washed three times with PBS at room temperature. Cells were stained with primary antibodies in blocking buffer for 30 min at 37°C. Samples were then washed three times with PBS again before staining with secondary antibodies for an additional 30 min at 37°C. Samples were washed three times with PBS and incubated with DAPI in PBS at room temperature for 10 min. Samples were then washed three times with PBS before being mounted and were subsequently examined with a Nikon A1 confocal microscope.

Immunoprecipitation

For coimmunoprecipitation involving cross-linking, cells after treatments were collected and washed twice in PBS. Cells were then cross-linked using 2 mM DSP at room temperature for 30 min; cross-linking was quenched by tris-HCl pH 7.4 at a final concentration of 20 mM. The cross-linked cells were then pelleted again by centrifuging at 1000*g* for 10 min and lysed in Flag lysis buffer containing 0.5% SDS. Cells were lysed on ice for 30 min and sonicated for 1 min to break down DNA. The lysate was then centrifuged at 13,000*g* for 30 min to collect supernatant. The supernatant was diluted so that the final concentration of SDS was 0.1%. The diluted cell lysate was subsequently used to bind anti-Flag M2 agarose overnight at 4°C. The Flag agarose was washed three times with 0.1% SDS-containing buffer before being eluted in Flag peptide (0.1 mg/ml) for 6 hours. The eluant was then denatured in 1× SDS protein loading buffer and subjected to Western blotting analysis.

Immunohistochemistry

For human brain sections, sections were deparaffinized, gradually rehydrated, and incubated for 10 min in 0.3% H_2O_2 diluted in methanol to quench endogenous peroxidase activity. For antigen retrieval, the sections were treated with 10 mM citric acid buffer (pH 6.0) and heated in a microwave oven. After three washes with PBS, the sections were incubated with an antibody directed against p-MLKL at a dilution of 1:50 and incubated overnight at 4°C. After three rinses with PBS, the sections were incubated with secondary antibody (EnVision+ System horseradish peroxidase, Dako) for 60 min at room temperature and subsequently exposed to the chromogen (3,3′ diaminobenzidine tetrachloride) system for 5 min. The sections were counterstained with hematoxylin, dehydrated, cleared, and coverslipped. Slides were examined and captured the images by light microscopy (Leica, Germany). Signal analysis was done with Leica Q550CW image analysis system (Germany) and QWin software. Signal was not detected in the negative control experiments including secondary antibody alone. The experiment was carried out in a double-blinded manner.

Statistical analysis

Statistical analysis was performed with Prism software (GraphPad). Cell death or cell survival rate was shown as means ± SD. Differences between means were assessed by two-way ANOVA with post hoc Tukey's test. Survival curves were compared using log-rank Mantel-Cox test.

SUPPLEMENTARY MATERIALS

stke.sciencemag.org/cgi/content/full/12/583/eaaw3423/DC1

Fig. S1. Translocation of phospho-MLKL onto lipid rafts upon TSZ treatment of HT-29 cells.

Fig. S2. The N-terminal helix bundle of MLKL was essential for its association with flotillins and for subsequent flotillin-mediated endocytosis.

Fig. S3. Four SNPs in the human *FLOT1* gene compromised the association between flotillin-1 and MLKL and sensitized cells to TSZ-induced necroptosis.

Fig. S4. Knockout of either *ALIX* or *SDCBP* in HT-29 cells enhanced necroptotic cell death.

Fig. S5. Concomitant knockout of *SDCBP* and *FLOT2* did not affect the TNFα signaling pathway.

Fig. S6. MLKL associated with TSG101, ALIX, and syntenin-1 through its N-terminal helix bundle.

Fig. S7. Knockout of *Flot2* but not of *Alix* or *Sdcbp* sensitized L929 cells to TZ-induced necroptosis.

Movie S1. *SDCBP* and *FLOT2* double-knockout cells were more sensitive to TSZ-induced necroptosis than wild-type HT-29 cells.

Data file S1. Mass spectrometry dataset for the phospho-MLKL affinity purification from lipid rafts in DSP–cross-linked cells.

REFERENCES AND NOTES

1. D. Brenner, H. Blaser, T. W. Mak, Regulation of tumour necrosis factor signalling: Live or let die. *Nat. Rev. Immunol.* **15**, 362–374 (2015).
2. P. Vandenabeele, L. Galluzzi, T. Vanden Berghe, G. Kroemer, Molecular mechanisms of necroptosis: An ordered cellular explosion. *Nat. Rev. Mol. Cell Biol.* **11**, 700–714 (2010).
3. J. M. Murphy, J. Silke, Ars Moriendi; the art of dying well - New insights into the molecular pathways of necroptotic cell death. *EMBO Rep.* **15**, 155–164 (2014).
4. S. Grootjans, T. Vanden Berghe, P. Vandenabeele, Initiation and execution mechanisms of necroptosis: An overview. *Cell Death Differ.* **24**, 1184–1195 (2017).
5. S. He, L. Wang, L. Miao, T. Wang, F. du, L. Zhao, X. Wang, Receptor interacting protein kinase-3 determines cellular necrotic response to TNF-alpha. *Cell* **137**, 1100–1111 (2009).
6. Y. Cho, S. Challa, D. Moquin, R. Genga, T. D. Ray, M. Guildford, F. K.-M. Chan, Phosphorylation-driven assembly of the RIP1-RIP3 complex regulates programmed necrosis and virus-induced inflammation. *Cell* **137**, 1112–1123 (2009).
7. D.-W. Zhang, J. Shao, J. Lin, N. Zhang, B.-J. Lu, S.-C. Lin, M.-Q. Dong, J. Han, RIP3, an energy metabolism regulator that switches TNF-induced cell death from apoptosis to necrosis. *Science* **325**, 332–336 (2009).
8. L. Sun, H. Wang, Z. Wang, S. He, S. Chen, D. Liao, L. Wang, J. Yan, W. Liu, X. Lei, X. Wang, Mixed lineage kinase domain-like protein mediates necrosis signaling downstream of RIP3 kinase. *Cell* **148**, 213–227 (2012).
9. J. M. Murphy, P. E. Czabotar, J. M. Hildebrand, I. S. Lucet, J.-G. Zhang, S. Alvarez-Diaz, R. Lewis, N. Lalaoui, D. Metcalf, A. I. Webb, S. N. Young, L. N. Varghese, G. M. Tannahill, E. C. Hatchell, I. J. Majewski, T. Okamoto, R. C. J. Dobson, D. J. Hilton, J. J. Babon, N. A. Nicola, A. Strasser, J. Silke, W. S. Alexander, The pseudokinase MLKL mediates necroptosis via a molecular switch mechanism. *Immunity* **39**, 443–453 (2013).
10. L. Su, B. Quade, H. Wang, L. Sun, X. Wang, J. Rizo, A plug release mechanism for membrane permeation by MLKL. *Structure* **22**, 1489–1500 (2014).
11. Z. Cai, S. Jitkaew, J. Zhao, H.-C. Chiang, S. Choksi, J. Liu, Y. Ward, L.-g. Wu, Z.-G. Liu, Plasma membrane translocation of trimerized MLKL protein is required for TNF-induced necroptosis. *Nat. Cell Biol.* **16**, 55–65 (2014).
12. X. Chen, W. Li, J. Ren, D. Huang, W.-t. He, Y. Song, C. Yang, W. Li, X. Zheng, P. Chen, J. Han, Translocation of mixed lineage kinase domain-like protein to plasma membrane leads to necrotic cell death. *Cell Res.* **24**, 105–121 (2014).
13. H. Wang, L. Sun, L. Su, J. Rizo, L. Liu, L.-F. Wang, F.-S. Wang, X. Wang, Mixed lineage kinase domain-like protein MLKL causes necrotic membrane disruption upon phosphorylation by RIP3. *Mol. Cell* **54**, 133–146 (2014).
14. C. N. Poston, E. Duong, Y. Cao, C. R. Bazemore-Walker, Proteomic analysis of lipid raft-enriched membranes isolated from internal organelles. *Biochem. Biophys. Res. Commun.* **415**, 355–360 (2011).
15. G. P. Otto, B. J. Nichols, The roles of flotillin microdomains – Endocytosis and beyond. *J. Cell Sci.* **124**, 3933–3940 (2011).
16. M. Amaddii, M. Meister, A. Banning, A. Tomasovic, J. Mooz, K. Rajalingam, R. Tikkanen, Flotillin-1/reggie-2 protein plays dual role in activation of receptor-tyrosine kinase/mitogen-activated protein kinase signaling. *J. Biol. Chem.* **287**, 7265–7278 (2012).
17. S. Bodin, D. Planchon, E. Rios Morris, F. Comunale, C. Gauthier-Rouviere, Flotillins in intercellular adhesion – From cellular physiology to human diseases. *J. Cell Sci.* **127**, 5139–5147 (2014).
18. C. Fork, J. Hitzel, B. J. Nichols, R. Tikkanen, R. P. Brandes, Flotillin-1 facilitates toll-like receptor 3 signaling in human endothelial cells. *Basic Res. Cardiol.* **109**, 439 (2014).
19. N. S. Imjeti, K. Menck, A. L. Egea-Jimenez, C. Lecointre, F. Lembo, H. Bouguenina, A. Badache, R. Ghossoub, G. David, S. Roche, P. Zimmermann, Syntenin mediates SRC function in exosomal cell-to-cell communication. *Proc. Natl. Acad. Sci. U.S.A.* **114**, 12495–12500 (2017).
20. J. Fares, R. Kashyap, P. Zimmermann, Syntenin: Key player in cancer exosome biogenesis and uptake? *Cell Adh. Migr.* **11**, 124–126 (2017).
21. Y. Choi, J.-H. Yun, J. Yoo, I. Lee, H. Kim, H.-N. Son, I.-S. Kim, H. S. Yoon, P. Zimmermann, J. R. Couchman, H.-S. Cho, E.-S. Oh, W. Lee, New structural insight of C-terminal region of Syntenin-1, enhancing the molecular dimerization and inhibitory function related on Syndecan-4 signaling. *Sci. Rep.* **6**, 36818 (2016).
22. M. F. Baietti, Z. Zhang, E. Mortier, A. Melchior, G. Degeest, A. Geeraerts, Y. Ivarsson, F. Depoortere, C. Coomans, E. Vermeiren, P. Zimmermann, G. David, Syndecan-syntenin-ALIX regulates the biogenesis of exosomes. *Nat. Cell Biol.* **14**, 677–685 (2012).
23. B. Strack, A. Calistri, S. Craig, E. Popova, H. G. Gottlinger, AIP1/ALIX is a binding partner for HIV-1 p6 and EIAV p9 functioning in virus budding. *Cell* **114**, 689–699 (2003).
24. A. J. Jimenez, P. Maiuri, J. Lafaurie-Janvore, S. Divoux, M. Piel, F. Perez, ESCRT machinery is required for plasma membrane repair. *Science* **343**, 1247136 (2014).
25. J. G. Carlton, J. Martin-Serrano, Parallels between cytokinesis and retroviral budding: A role for the ESCRT machinery. *Science* **316**, 1908–1912 (2007).

26. T. Yoshimori, A. Yamamoto, Y. Moriyama, M. Futai, Y. Tashiro, Bafilomycin A1, a specific inhibitor of vacuolar-type H^+-ATPase, inhibits acidification and protein degradation in lysosomes of cultured cells. *J. Biol. Chem.* **266**, 17707–17712 (1991).
27. G. P. Solis, M. Hoegg, C. Munderloh, Y. Schrock, E. Malaga-Trillo, E. Rivera-Milla, C. A. O. Stuermer, Reggie/flotillin proteins are organized into stable tetramers in membrane microdomains. *Biochem. J.* **403**, 313–322 (2007).
28. P. Garcia, R. Gupta, S. Shah, A. J. Morris, S. A. Rudge, S. Scarlata, V. Petrova, S. McLaughlin, M. J. Rebecchi, The pleckstrin homology domain of phospholipase C-delta 1 binds with high affinity to phosphatidylinositol 4,5-bisphosphate in bilayer membranes. *Biochemistry* **34**, 16228–16234 (1995).
29. C. A. Homewood, D. C. Warhurst, W. Peters, V. C. Baggaley, Lysosomes, pH and the anti-malarial action of chloroquine. *Nature* **235**, 50–52 (1972).
30. S. Yoon, A. Kovalenko, K. Bogdanov, D. Wallach, MLKL, the protein that mediates necroptosis, also regulates endosomal trafficking and extracellular vesicle generation. *Immunity* **47**, 51–65.e7 (2017).
31. S. Zargarian, I. Shlomovitz, Z. Erlich, A. Hourizadeh, Y. Ofir-Birin, B. A. Croker, N. Regev-Rudzki, L. Edry-Botzer, M. Gerlic, Phosphatidylserine externalization, "necroptotic bodies" release, and phagocytosis during necroptosis. *PLOS Biol.* **15**, e2002711 (2017).
32. Y.-N. Gong, C. Guy, H. Olauson, J. U. Becker, M. Yang, P. Fitzgerald, A. Linkermann, D. R. Green, ESCRT-III acts downstream of MLKL to regulate necroptotic cell death and its consequences. *Cell* **169**, 286–300.e16 (2017).
33. V. Bitsikas, K. Riento, J. D. Howe, N. P. Barry, B. J. Nichols, The role of flotillins in regulating aβ production, investigated using *flotillin* 1-/-, *flotillin* 2-/- double knockout mice. *PLOS ONE* **9**, e85217 (2014).
34. L. Duprez, N. Takahashi, F. van Hauwermeiren, B. Vandendriessche, V. Goossens, T. vanden Berghe, W. Declercq, C. Libert, A. Cauwels, P. Vandenabeele, RIP kinase-dependent necrosis drives lethal systemic inflammatory response syndrome. *Immunity* **35**, 908–918 (2011).
35. Y. Ren, Y. Su, L. Sun, S. He, L. Meng, D. Liao, X. Liu, Y. Ma, C. Liu, S. Li, H. Ruan, X. Lei, X. Wang, Z. Zhang, Discovery of a highly potent, selective, and metabolically stable inhibitor of receptor-interacting protein 1 (RIP1) for the treatment of systemic inflammatory response syndrome. *J. Med. Chem.* **60**, 972–986 (2017).
36. A. Caccamo, C. Branca, I. S. Piras, E. Ferreira, M. J. Huentelman, W. S. Liang, B. Readhead, J. T. Dudley, E. E. Spangenberg, K. N. Green, R. Belfiore, W. Winslow, S. Oddo, Necroptosis activation in Alzheimer's disease. *Nat. Neurosci.* **20**, 1236–1246 (2017).
37. A. M. Cataldo, D. J. Hamilton, R. A. Nixon, Lysosomal abnormalities in degenerating neurons link neuronal compromise to senile plaque development in Alzheimer disease. *Brain Res.* **640**, 68–80 (1994).
38. L. S. Whyte, A. A. Lau, K. M. Hemsley, J. J. Hopwood, T. J. Sargeant, Endo-lysosomal and autophagic dysfunction: A driving factor in Alzheimer's disease? *J. Neurochem.* **140**, 703–717 (2017).

Acknowledgments: We would like to express our gratitude to the members from the animal facility, the flow cytometry facility, the imaging facility, and the oligonucleotide synthesis facility at National Institute of Biological Sciences. We thank Z. Ying for technical assistance with the animal experiment. We thank J. H. Snyder for critically reading the manuscript. **Funding**: This work was supported by National Basic Science 973 grant no. 2010CB835400 from the Chinese Ministry of Science and Technology. W.F. was supported by an Amgen-China postdoctoral fellowship from 2014 to 2018. **Author contributions**: W.F. and X.W. designed the research and analyzed the data. W.F., J.G., B.G., W.Z., and L. Ling carried out all cell-based experiments. T.X. did the animal experiment. C.P. helped generate the *Flot1* and *Flot2* double-knockout mice. L. Li and S.C. carried out mass spectrometry analysis. H.W. and J.Z. did the human Alzheimer's disease study. W.F. and X.W. wrote the manuscript. **Competing interests**: The authors declare that they have no competing interests. **Data and materials availability**: The mass spectrometry proteomics data have been deposited at the ProteomeXchange Consortium (www.ebi.ac.uk) under the project title "Phospho-MLKL protein complex purified from human HT-29 cell," dataset identifier PXD012685. All other data needed to evaluate the conclusions in the paper are present in the paper or the Supplementary Materials. Cell lines and *Flot* knockout mice used in this study require a material transfer agreement from the National Institute of Biological Sciences, Beijing, China. Other materials used in this work are available from the corresponding author upon reasonable request.

Submitted 11 December 2018
Accepted 8 May 2019
Published 28 May 2019
10.1126/scisignal.aaw3423

Citation: W. Fan, J. Guo, B. Gao, W. Zhang, L. Ling, T. Xu, C. Pan, L. Li, S. Chen, H. Wang, J. Zhang, X. Wang, Flotillin-mediated endocytosis and ALIX–syntenin-1–mediated exocytosis protect the cell membrane from damage caused by necroptosis. *Sci. Signal.* **12**, eaaw3423 (2019).

Science Signaling

Flotillin-mediated endocytosis and ALIX–syntenin-1–mediated exocytosis protect the cell membrane from damage caused by necroptosis

Weiliang Fan, Jia Guo, Beichen Gao, Wenbin Zhang, Liucong Ling, Tao Xu, Chenjie Pan, Lin Li, She Chen, Hua Wang, Jing Zhang and Xiaodong Wang

Sci. Signal. **12** (583), eaaw3423.
DOI: 10.1126/scisignal.aaw3423

Exit the necroptosis executioner

In cells dying by necroptosis, the pseudokinase MLKL becomes phosphorylated and competent to rupture the plasma membrane. However, the appearance of phosphorylated MLKL does not always lead to necroptosis, prompting Fan *et al.* to investigate how the activity of this necroptosis executioner is suppressed. They found that phosphorylated MLKL could be directed by flotillin-1 and flotillin-2 into lipid rafts and, subsequently, lysosomes. In addition, phosphorylated MLKL could be ejected from cells in exosomes in a pathway dependent on the ESCRT proteins ALIX and syntenin-1. These mechanisms may be safeguards to ensure that only signals of sufficient intensity induce necroptosis.